Mon. Not. R. Astron. Soc. **000**, 000–000 (0000) Printed 10 April 2000 (MN LaTeX style file v1.4)

Polarimetry and spectroscopy of RXJ1141.3-6410: a single pole AM Her system

David A. H. Buckley[1,2], Mark Cropper[3], Kurt van der Heyden[1,4],
S.B. Potter[3,1] & Dayal T. Wickramasinghe[2]

[1] *South African Astronomical Observatory, P O Box 9, Observatory, Observatory 7935, South Africa*
[2] *The Astrophysical Theory Centre, School of Mathematical Sciences, The Australian National University, Canberra, ACT 0200, Australia*
[3] *Mullard Space Science Laboratory, University College London, Holmbury St. Mary, Dorking, Surrey RH5 6NT, United Kingdom*
[4] *Department of Astronomy, University of Cape Town, Rondebosch 7700, South Africa*

Received:

ABSTRACT

We present polarimetric and spectroscopic observations of the ROSAT source RX J1141.3-6410, recently identified as a polar. The detection of circular polarisation variations, with an amplitude of 10 percent, over a 3.16 h period confirms that the system is a polar (AM Herculis star). Supporting evidence comes from the nature of the emission lines and their radial velocity variability. In addition, we observe continuum slope changes in the far red spectral region (∼6000–8200Å), indicative of phase dependent cyclotron emission. Polarimetric modelling at two wavelengths establishes RX J1141.3–6410 as a single-pole system, with $i \sim \beta \sim 70°$. The accretion region is extended in magnetic longitude, and is totally self-occulted for ∼25% or the orbit. The radial velocity curves derived from the emission lines show a phasing with maximum blueshift occuring with $\Delta\phi \sim 0.05$ of maximum intensity and circular polarization. In addition, the broader component of the lines exhibit a substantial radial velocity phase shift with respect to the narrower component, in the sense that the broad component preceeds the narrow. This can be readily understood if the narrower component is principally due to orbital motion of the stream material and the broad component mainly due to streaming motion near the coupling region. The phasing of the CaII near-IR line radial velocities also supports this general picture.

Key words: binaries: close – stars: individual: RXJ1141.3–6410 – novae, cataclysmic variables – X-rays: stars – polarization.

1 INTRODUCTION

New magnetic cataclysmic variables, and in particlar the synchonized polar (AM Herculis) sub-class, continue to be found from the *ROSAT* surveys and from serendipitous pointed observations. RXJ1141.3–6410 was selected by Motch et al. (1996) for further study in their Galactic plane sample on the basis of its soft X-ray spectrum. They identified it with a $V \sim 16.5$ star with strong HeIIλ4686 emission lines in its spectra, and this, together with the X-ray hardness ratios, led them to suggest that the star is an AM Her system (see Warner 1995, Cropper 1990 for reviews). Cieslinski & Steiner (1997) established a photometric period of 3h 09m, fairly typical of that for AM Her systems. Later Rodrigues, Cieslinski & Steiner (1998) obtained follow up polarisation (circular only) and spectroscopy confirming its membership of the class. Here we present further polarimetric observations (including linear) and spectroscopic observations and investigate its nature in more detail.

2 OBSERVATIONS

2.1 Polarimetry

The polarimetric observations were made with the University of Cape Town Polarimeter (UCTP; Cropper 1985) on the 1.9m telescope at the Sutherland site of the South African Astronomical Observatory (SAAO). The observations were taken in 1996 February 15 and March 21–25. The UCTP was configured in the simultaneous linear and circular polarimetry and photometry mode. A white light bandpass $(3500 - 9000\text{Å})$ defined by an RCA31034A GaAs photomultiplier response was used for some of the observations. For others a broad blue band $(3500 - 5500\text{Å})$, defined by a BG39

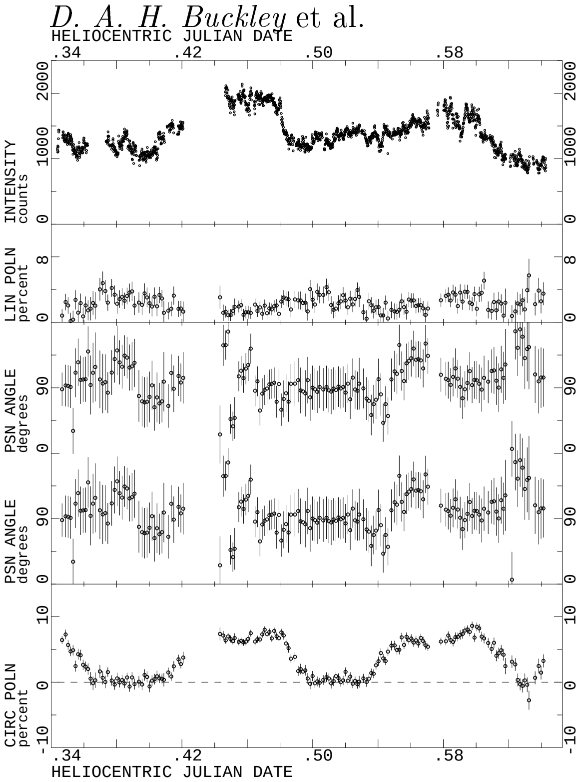

Figure 1. White-light polarimetry taken on 1996 March 21/22 (times in HJD - 2450164)

Run	Date	HJD start	Duration (min)	Filter
1	1996 February 15/16	2450129.560	95	white
2	1996 March 21/22	2450164.346	426	white
3	1996 March 22/23	2450165.292	508	BG39
4	1996 March 22/23	2450165.292	508	OG570
5	1996 March 23/24	2450166.372	383	V
6	1996 March 23/24	2450166.395	352	R_c
7	1996 March 24/25	2450167.273	283	V
8	1996 March 24/25	2450167.273	283	I_c
9	1996 March 25/26	2450168.385	253	BG39
10	1996 March 25/26	2450168.385	253	OG570

Table 1. Log of the polarimetric observations taken at SAAO.

filter, and a broad red band ($5700-9000$Å), defined by an OG570 filter, were used. There were also short runs in the V, R_c and I_c bands to constrain the polarisation continuum spectrum. A log of these observations is given in Table 1.

The observations were at times taken under non-photometric conditions. These intervals have been excised from the photometric data, and also from the polarisation data when increased uncertainties in the data indicate that they have been substantially affected. The white light data from Run 2 are shown in Fig. 1. We searched our white light, OG570 and R_c band data for periodicities in the range up to 40 cycles/day. This found a single periodicity at 0.13152(7) days (uncertainty in last digit in parentheses), consistent with the more precise value of 0.131517(3) days reported by Cieslinski & Steiner (1997). We have therefore used Cieslinski & Steiner (1997) to phase our observations. The data were then folded on this ephemeris averaged into phase bins and plotted as a function of phase. The average behaviour in the BG39 and OG570 bands are shown in Figures 2(a) and (b). The figures show the light curve (on a linear scale) in the top panel, followed on the panels below by the linear polarization, its position angle, and the circular polarization at the bottom. The position angle is plotted twice vertically for continuity and the binned curves are repeated over two phases for clarity.

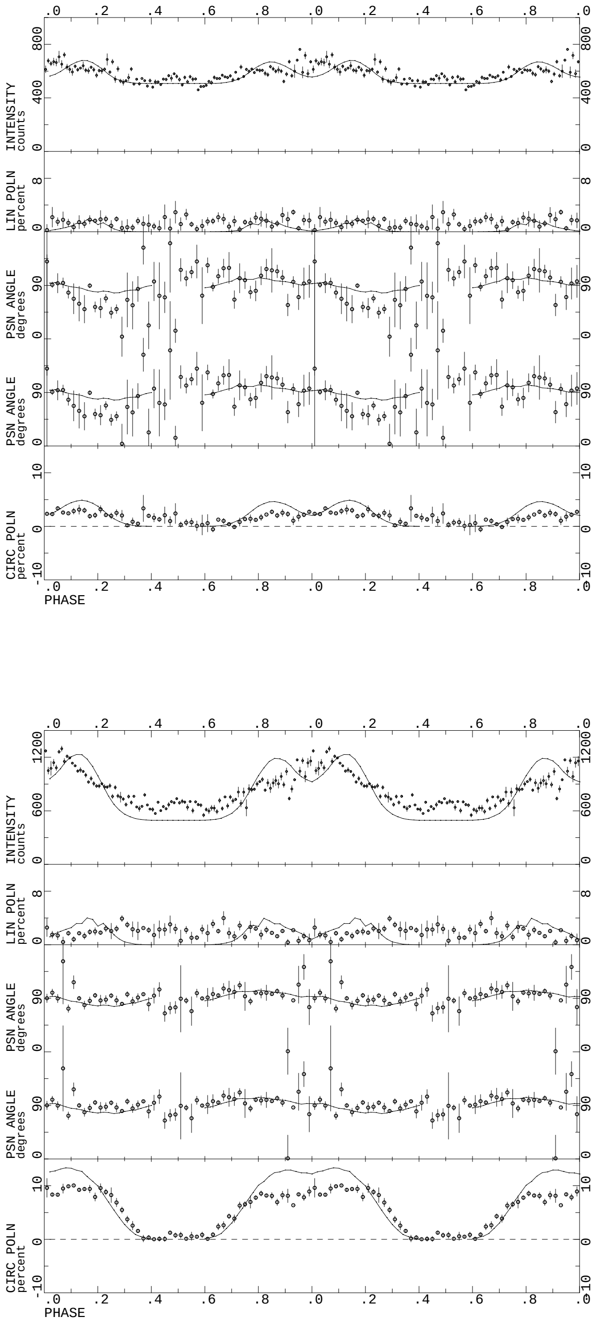

Figure 2. Phase-binned polarisation of RXJ1141.3–6410 in (a) blue (BG39) and (b) red (OG570) bands. Overlaid are the model fits (see text).

2.2 Spectroscopy

Time resolved spectroscopy of RX J1141.3–6410 was taken on two occasions, 1996 April 20 and 1998 March 29/30. The 1996 observations used the Double Beam Spectrograph (DB-S) on the Australian National University's 2.3-m telescope at Siding Spring Observatory (SSO). The 'red' and 'blue' arms of the spectrograph covered the region 3400–6000Å and 5500–8200Å at a reciprocal dispersion of 2Å pixel^{-1}. The observations were obtained with a slit matching the seeing size ($\sim$ 1 arcsec FWHM) and rotated to the parallactic angle, thus minimizing atmospheric dispersion effects. Comparison arc (Cu-Ar) spectra were taken at regular intervals (every $\sim$ 1200 s) during the observation. Bias and flat field frames were taken at the beginning and the end of the night.

Spectra of RX J1141.3–6410 were obtained, mostly with 300 s exposures, from HJD 2450193.929 to HJD 2450194.092, amounting to a phase coverage of 1.24. Following the wavelength calibration, we normalized all the spectra by a smoothed high S/N ratio spectrum of the featureless DF white dwarf, EG 131. This procedure (Bessell 1996) has the effect of removing both the telluric absorption lines (e.g. the B-band) and removing the sensitivity variations introduced into the spectra by the beamsplitting dichroic filter. An observation of the spectrophotometric standard LTT6248, normalized in exactly the same manner, was then used to flux calibrate the data. In Fig. 3 we show the mean combined red/blue spectrum of RX J1141.3-6410. This spectrum is typical of an AM Her system, with Balmer, HeI and, most significantly, strong HeII emission lines. The Balmer jump is also seen in emission, while at some phases the continuum flux increases towards longer wavelength. This latter point is discussed in detail in a later section (section 5).

The 1998 March 29/30 observations were made at SAAO using the Cassegrain spectrograph on the 1.9-m telescope and utilizing the SITe1 CCD (1752 × 266 × 15μm pixels). Spectra were obtained, with 900-s exposures from HJD 2450902.3812 to HJD2450902.5424, giving a coverage of $\sim$1.2 orbital cycles. We used Grating 7 (300 l mm^{-1}) at an angle that extended the wavelength coverage in the red: from 5400–9200Å at a resolution of $\sim$5Å. We used a wide slit to reduce slit losses, and took spectra of smooth-spectrum (i.e. featureless) and flux standards at a similar airmass to RX J1141.3–6410 before and after the observations. Our reduction procedure, following wavelength calibrations, consisted, as above, of removing the Telluric lines and fringe features (in the far red) by dividing the data with a normalised high signal–to–noise ratio spectrum of the smooth spectrum standard, suitably adjusted so that stellar features of the star were not introduced. Finally, the flux standard (treated in an identical manner) was used to calibrate the RX J1141.3–6410 spectra onto an absolute flux scale.

Our main purpose for these observations was extending the red end in order to investigate the behaviour of the cyclotron flux. This is discussed in a later section.

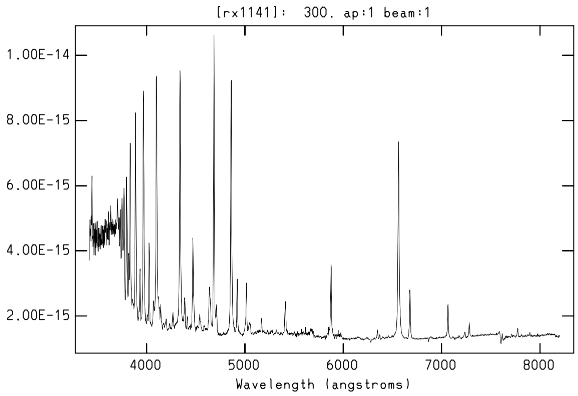

Figure 3. Mean combined red-blue spectrum of RX J1141.3–6410

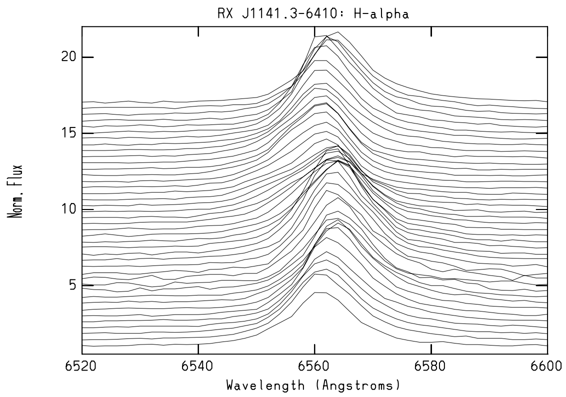

[t]

Figure 4. Trailed H-α profile of RX J1141.3–6410 showing velocity and width changes. Time increases upwards, and the spectra cover $\sim$1.3 orbital cycles.

3 EMISSION LINES AND RADIAL VELOCITIES

The structure of the emission lines is typical of a polar. The lines show a strong pseudo-Gaussian core component, together with broad wings which extend $\sim$1000 km s^{-1} from the line centre. Both the line positions, widths and fluxes are seen to vary over the orbital period, as evident in the Hα line, shown in Fig. 4.

We made Gaussian fits to the emission lines in the 1996 SSO data, and in Fig. 5 we plot the resulting line widths and fluxes. Rather than adopting radial velocities from the Gaussian fits, we determined them using a Gaussian convolution scheme (Schneider and Young 1980; Shafter 1985), which is more appropriate for blended, multi-velocity component, lines.

Eight Gaussian 'filters' were used (e.g. Buckley & Tuohy 1990), with separations of 2000, 1500, 1200, 900, 700, 500, 200 and 100 km s^{-1} , and corresponding Gaussian sigmas of 400, 250, 200, 200, 200, 200, 200 and 100 km s^{-1} . For each of the radial velocity curves we used a least-squares sine fitting algorithm to determine the amplitude (K-velocity), zero level (γ-velocity) and phase (ϕ_0; with respect to the ephemeris of Cielinski & Steiner 1997). In Fig. 6 we show a sample of three radial velocity curves for the Hα line, together with their best-fit sinusoids.

We convolved the three strongest Balmer lines (Hα, β, γ) in this manner, plus the HeI line λ4471Å and HeII λ4685Å. The three variable parameters (K, γ, ϕ_0) are

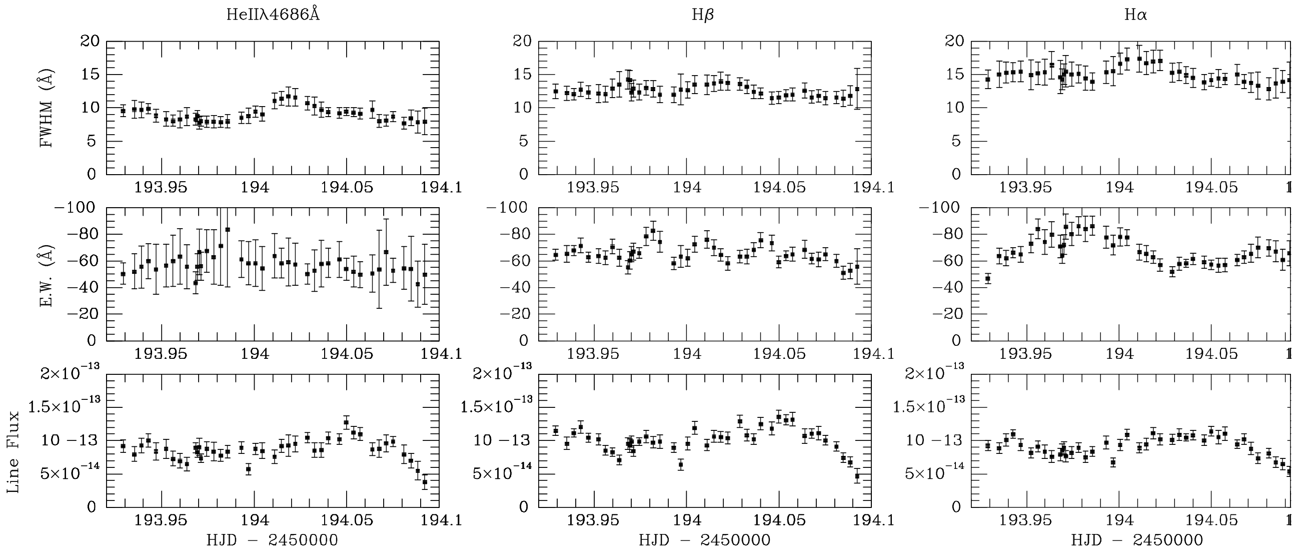

Figure 5. Parameters for Gaussian fits to HeII λ4686Å, Hβ and Hα.

plotted in Fig. 7 for the Balmer lines (Hγ, Hβ and Hα) and in Fig. 8 for the helium lines (HeI λ4471Å and HeII λ4686Å).

We see that the K-velocity increases into the wings, and converges to a value of ~200 km s^{-1} . For the Balmer lines, the wings extend at least to ~1000 km s^{-1}from line centre, but the HeII λ4686Å line can only be traced to ~600 km s^{-1} from it rest velocity. In addition, we find a trend of an increasingly negative γ-velocity (ie. blue-shifted) for the Balmer lines as we move into the wings. There is also some indication of a slight phase shift as a function of the Gaussian separation, particularly in the case of Hα.

Figure 9 shows the radial velocities of the CaII $\lambda 8498 \mathring{A}$ emission line as a function of orbital phase. Using a least-squares sine fitting algorithm we find maximum blue shift occurs at phase ~ 0.4 placing it ~ 0.3 in phase later than the maximum blue shift of the balmer lines. It has a zero level (γ-velocity) of ~17km s^{-1} in agreement with the value derived by Rodrigues, Cieslinski & Steiner (1998) for the narrow component of H-α.

4 CONSTRAINTS FROM THE LIGHT AND POLARIZATION CURVES

The intensity data in Figs 1 and 2 show that there is a single main source of polarised emission from the system, seen optimally at $\phi \sim 0.0$. Values of zero for the circular polarisation between $\phi \sim 0.35 - 0.6$ indicates that this source is out of view at these phases. At other phases the circular polarisation is positive and relatively constant at ~ 8 per cent in the red band and ~ 3 per cent in the blue band. The linear polarisation is low at all phases and the position angle is relatively constant, particularly in the red-band data in Fig. 2(b). Most of the polarised emission is at red wavelengths.

The small variation in position angle in this system provides strong constraints on the location of the cyclotron emission region. The position angle, and hence the projected orientation of the accreting field lines, is the same at the beginning and end of the bright phase. This can be satisfied only if the system is viewed almost from the orbital plane $\iota \simeq 90^\circ$ and if the orientation of the magnetic pole is also almost in the orbital plane ($\beta \simeq 90^\circ$, fig 10a). With these orientations, the position angle will remain constant as the white dwarf rotates, before switching almost instantaneously through 180° (*i.e.* it appears the same) at the centre of the bright phase and remaining at this value until the emission region disappears. There is no evidence for any eclipse in this system, either from our data or that of Cieslinski & Steiner (1997) and Rodrigues, Cieslinski & Steiner (1999), so that the maximum $\iota \sim 70^\circ$. The small range of position angle variation can be maintained, however, by allowing the emission region to be displaced from the magnetic pole and allowing the pole to lie slightly out of the orbital plane. Thus we have adopted $\iota \simeq \beta \simeq 70^\circ$ (fig 10a).

At these orientations a point source emission region will be in view for only slightly longer than $0.5P_{orb}$. In order to extend the bright phase, and the duration of non-zero circular polarisation to $\sim 0.75P_{orb}$, the emission region has to be spatially, or vertically, extended on the surface of the white dwarf. For simplicity in our polarisation modelling we neglect the possible vertical extent of the emission region and we follow the example of others (Wickramasinghe et al. 1991, Ramsay et al. 1996) in extending the emission region into an arc.

With these constraints in mind we have modelled the emission from an accretion arc using the technique described in Ramsay et al. (1996). This uses as a basis the single temperature models of Wickramasinghe & Meggitt (1985), and takes into account the effect of non-radial accretion down magnetic field lines in a dipole geometry and the effects of magnetic field spread. The model was a constant temperature 10 keV model. We have experimented in the placing of the emission points and find that an arc located approximately at the footpoints of magnetic fieldlines which would accrete from a region of constant radius from the white dwarf reproduces the observations moderately well. The arc is shown in Figs. 10a and b. The centre of the arc is lower in white dwarf latitude than the magnetic pole, while the ends of the arc wrap around the magnetic pole to lower

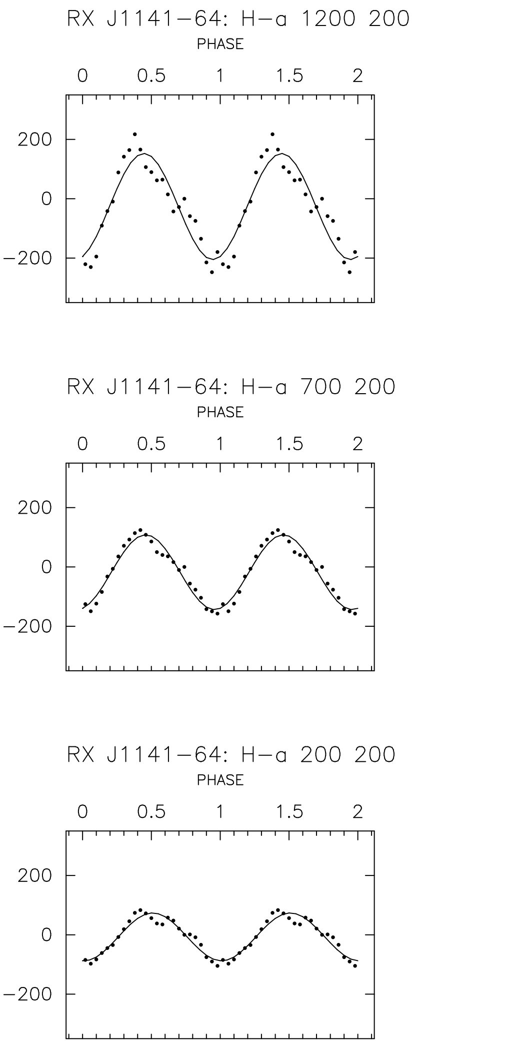

Figure 6. Three radial velocity curves for Hα determined using the Gaussian convolution method for separations of 1200, 700 and 200 km s^{-1} , and $\sigma = 200$ km s^{-1} .

magnetic latitudes (magnetic latitude runs from the upper magnetic pole 0^{o} to the lower magnetic pole 180^{o}). The arc is necessary not only to extend the bright phase, but also to render the circular polarisation variation more flat-topped. We proceeded initially by concentrating on the OG570 data in Fig. 2(b). We experimented by modifying the length of the arc, its proximity to the pole and its curvature, but we have assigned equal accretion rates in each spatial element of the arc. We have been able to reproduce the main features of the light and polarisation data with our model, which, even without an automated procedure to optimise the fit, we believe is relatively well optimised. It should be made clear, however, that it is not possible to exclude other configurations which might produce similarly good fits, but we believe the constraints noted above make this unlikely except in detail.

We permitted a constant dilution factor of unpolarised light, in order to account for the emission from other structures in the binary, such as the accretion stream and stellar

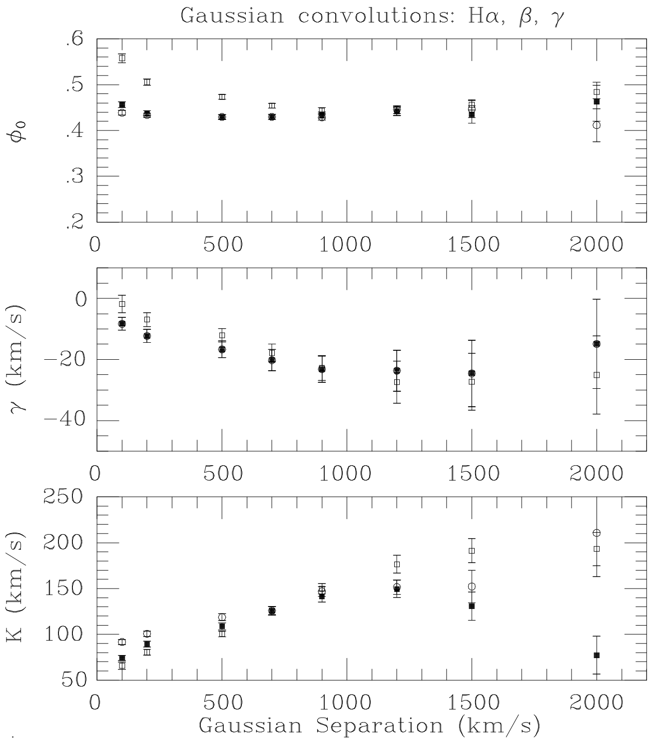

Figure 7. Variation in the Balmer line radial velocity parameters, K, γ and ϕ_0, determined from the Gaussian convolution technique, as a function of the separation of the Gaussian 'filters' (Symbols: Hα empty box, Hβ filled box, Hγ circle).

photospheres. We have used the same model in both OG570 and BG39 bands, with approximately the same diluting flux to produce the two fits in Fig. 2. The fit is sensitive to the polar magnetic field, which we find to be $\sim$ 20 MG and to the value of the optical depth parameter Λ (Wickramasinghe & Meggitt 1985), for which we adopted a value of 10^5.

5 SPECTRAL SLOPE CHANGES: EVIDENCE OF CYCLOTRON EMISSION

Since their discovery (Visvanathan and Wickramsinghe 1979), cyclotron emission lines from the post-shock accretion column have been used in determining magnetic field of $\sim$14 polars (Bailey 1995). Cyclotron harmonics are sometimes manifested as broad 'humps' in their spectra, often quite subtle and difficult to detect. Spectra need to be very carefully reduced and flux calibrated in order that atmospheric and instrumental effects are removed entirely.

The techniques we used to flux calibrate our spectra is discussed above. We did not detect any cyclotron hump structure in our spectra. However, the trailed spectra in Figs. 11a and c show that there are changes in the spectral slope over the orbital period, indicative of cyclotron emission. In particular the cyclotron spectra rises and peaks at $\sim$8000Å with increasing intensity during the bright phase. The spectra then begins to decrease longward of $\sim$8000Å as seen in the SAAO observations fig. 11c.

Fig. 11b shows the predicted cyclotron model spectra produced by the emission region that was constructed in order to model the observed polarimetric observations. The

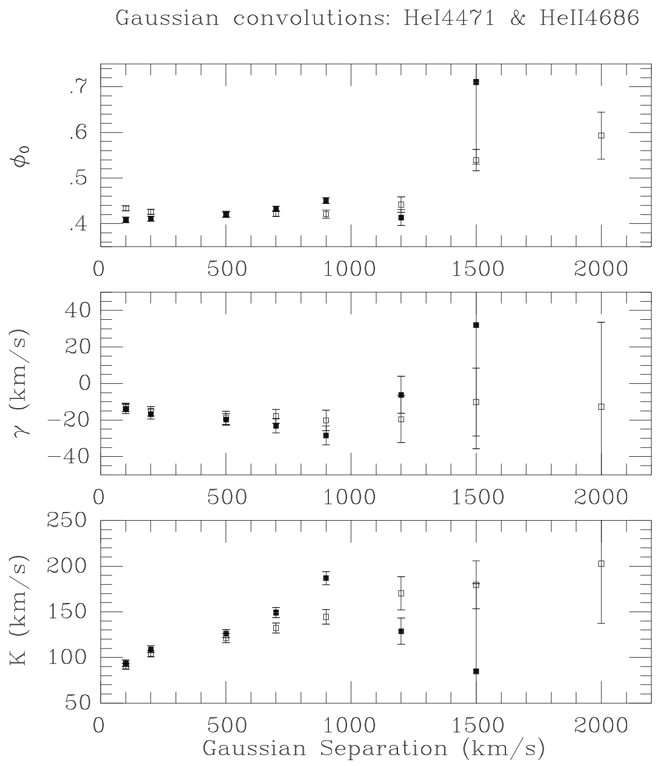

Figure 8. Variation in the HeI (empty sqaures) and HeII (filled sqaures) line radial velocity parameters, K, γ and ϕ_0, determined from the Gaussian convolution technique, as a function of the separation of the Gaussian 'filters'.

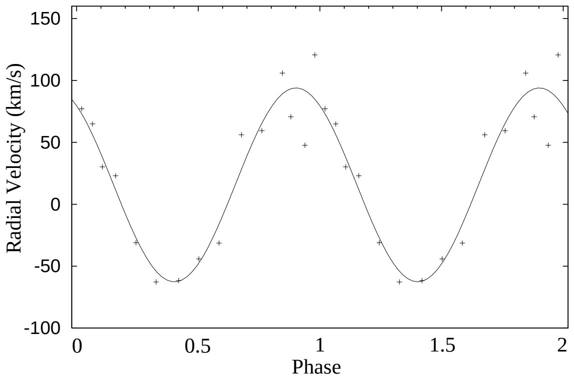

Figure 9. Radial velocity measurements of the CaII emission line.

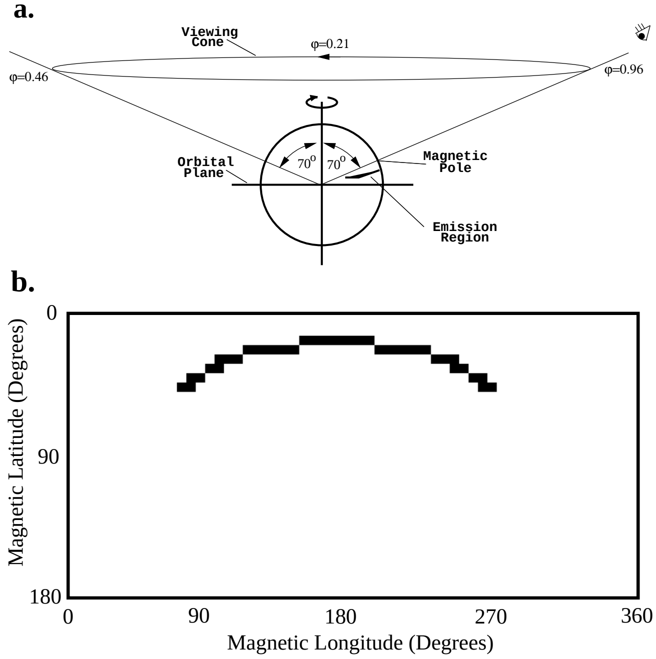

Figure 10. (a) The viewing geometry of the model used in section 5. (b) The arc used in modelling the cyclotron emission in Fig. 2.

model uses the same parameters that were used to reconstruct the broad band polarimtric observations presented in section 4. The model predicts the overall bright and faint emission as seen in the SSO and SAAO spectra with the intensity rising towards the red wavelengths. The model also predicts an absorption dip at approximately phase 0.0 which becomes less prominant and indeed rises to maximum flux at $\sim$8000Å . There is an indication of such a dip in the trailed spectra of fig 11a and in the white light circular polarization variations shown in fig 1. The dip is caused by self absorption of the cyclotron emission as the emission region is viewed parallel to the magnetic field lines that feed it.

6 DISCUSSION

The behavior of the radial velocity and polarimetric data provide a consistent picture of the line emitting gas free-falling in a curved, accelerating accretion stream.

The relative phasing of the radial velocity and intensity/polarisation curves is typical of polars: maximum redshift of the H-α occurs at $\phi \sim 0.45$ (eg. in Figs 7), while the accretion region is seen most face on at $\phi \sim 0.0$ (Figs 2 and 10). This means that the maximum blueshift occurs 0.05 of a period before the accretion region is seen face on. The CaII $\lambda 8498\AA$ emission line is generally associated with the irradiated face of the secondary. It has maximum blue shift at phase ~ 0.4 which places the accretion region $\sim 145^{\circ}$ ahead of the line of centers.

The broad emission line component seen in the H-α data (Fig. 7) leads the narrow component by 0.1P$_{orb}$. This is consistent with emission from material dominated by streaming velocities (Liebert & Stockman 1985): maximum blueshift would be expected to be at $\phi = 0.0$, so that the $\sim$ 0.1P$_{orb}$ delay in phase indicates that the stream is curving backwards from the radial direction towards the part of the stream that is dominated by orbital motions and the expected (from the CaII $\lambda 8498\AA$ emission line) position of the secondary.

The small negative γ velocities indicate that (for an accretion region in the upper hemisphere) the streaming velocities out of the plane occur near the threading region,

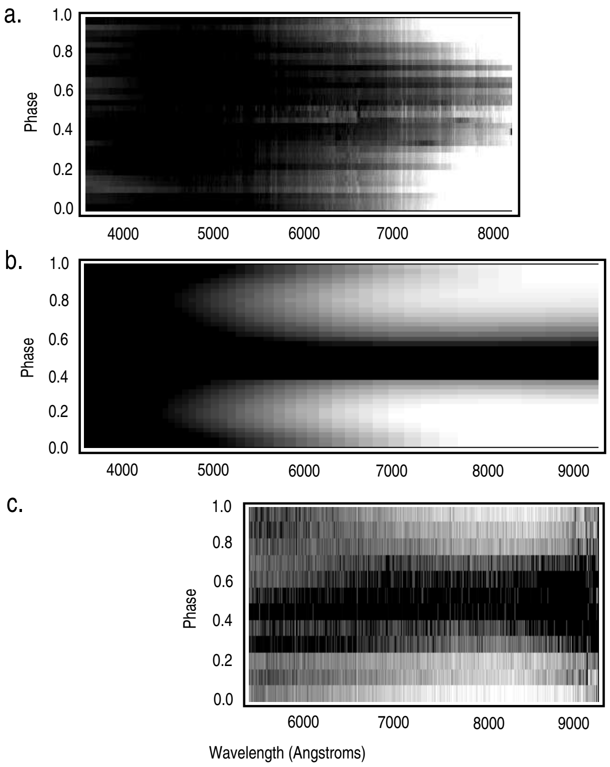

Figure 11. (a) SSO trailed spectra with emission lines removed. (b) Model trailed cyclotron spectra (see text). (c) SAAO trailed spectra with emission lines removed.

rather than near the white dwarf surface. The measured K velocity amplitude (Fig. 7) of the narrow component is also consistent with a location closer to the secondary.

Rodrigues et al give a lower inclination to explain the low radial velocities that they measured. Our polarimetric modelling suggests an orbital inclination of $\iota \sim 70^{\circ}$. However, where other model configurations might produce similarly good fits, we believe the constraints dereived from the polarimetry make this unlikely except in detail.

ACKNOWLEDGEMENTS

We are grateful to the Director, Dr R. Stobie, for the generous allocation of telescope time at SAAO.

REFERENCES

Bailey, J. A., 1995,Cape Workshop on Magnetic cataclysmic variables; Astronomical Society of the Pacific Conference Series, Volume 85, Proceedings of the Cape Workshop, held in Cape Town, 23-27 January 1995, San Francisco: Astronomical Society of the Pacific (ASP), edited by D.A.H. Buckley and B. Warner, p.10

Bessell, M., 1996, *Private Communication*

Buckley, D. A. H., Tuohy, I. R., 1990, ApJ 349, 296

Cropper, M. S., 1985, MNRAS, 212, 719

Cropper, M. S., 1988, MNRAS, 231, 597

Cropper, M. S., 1990, Sp. Sci. Rev., 54, 195

Cieslinski, D., Steiner, J. E., 1997, MNRAS, 291, 321

Liebert, J., Stockman, H. S., 1985, In: Lamb D. Q., Patterson J. (eds.) Cataclysmic Variables and low mass X-Ray binaries, D. Reidel Publ. Co., Dordrecht, p. 151

Motch, C., Haberl, F., Guillout, P., Pakull, M., Reinsch, K., Krautter, J., 1996, A&A, 307, 459

Ramsay, G., Cropper, M., Wu, K., Potter, S., 1996, MNRAS, 282, 726

Rodrigues, C. V., Cieslinski, D., Steiner, J. E., 1998, A&A, 335, 979

Schneider, Young, 1980, ApJ 238, 946

Shafter, A. W., 1985, In: Lamb D. Q., Patterson J. (eds.) Cataclysmic Variables and low mass X-Ray binaries, D. Reidel Publ. Co., Dordrecht, p. 355

Visvanathan, N, Wickramasinghe, D. T., 1979, Nature, 281, 47

Warner, B., 1995. Cataclysmic Variable Stars. Cambridge Univ. Press, Cambridge

Wickramasinghe, D. T., Bailey, J. A., Meggitt, S. M. A., Ferrario, L., Hough, J., Tuohy, I. R., 1991, MNRAS, 251, 28

Wickramasinghe, D. T., Meggitt, S. M. A., 1985, MNRAS, 214, 605